Evaluation of Horizontal to Vertical Spectral Ratio and Standard Spectral Ratio Methods for Mapping Shear Wave Velocity Across Anchorage, Alaska

Authors: John D. Thornley[a,b], Utpal Dutta[c], John Douglas[a], Zhaohui (Joey) Yang[c]

a. University of Strathclyde, Glasgow, Department of Civil and Environmental Engineering, James Weir Building, Level 5, 75 Montrose Street, Glasgow, G11XJ (UK)
b. Golder Associates Inc., 1701 Oxford Drive, Anchorage, Alaska 99503 (USA)
c. University of Alaska, Anchorage, Department of Civil Engineering. 3211 Providence Drive, EIB, Anchorage, Alaska 99508 (USA)

Corresponding Author: John Thornley (john_thornley@golder.com)

ORCID ID: 0000-0001-6583-3562

Abstract

The use of horizontal to vertical spectral ratios (HVSR) of earthquake ground motions has become a standard technique to characterize sites, especially those lacking subsurface measurements. Several studies have developed relationships between HVSR results and time-averaged shear-wave velocity in the upper 30m (V_{S30}). Other studies have utilized standard spectral ratios calculated from horizontal ground motion Fourier amplitude spectra to estimate V_{S30}. Anchorage, Alaska (USA), has a network of strong-motion recording stations, many of which have no site-specific subsurface characterization. This study compares measured V_{S30} and HVSR results from 18 strong-motion stations to four regional models developed by others. A relationship between the 1 Hz band-averaged (0.5 to 2.5 Hz) spectral amplification results and V_{S30} is presented. V_{S30} estimates for the strong-motion stations are made, and a regional model is developed between HVSR and V_{S30}, both in terms of f_{peak} (the frequency of the peak HVSR amplitude) and A_{peak} (the amplitude of the peak). In addition to the regional model, additional V_{S30} data from other sites in Anchorage, including 19 downhole V_{S30} measurements and 22 microtremor V_{S30} estimates from others, are used with the strong-motion station V_{S30} estimates to develop a V_{S30} contour map of Anchorage. The contouring represents the spatial distribution of the site classes of the local building code, which are based on V_{S30}. This map may be incorporated into planning documents for future developments in the city.

Key Words

Horizontal to Vertical Spectral Ratio, Standard Spectral Ratio, Shear Wave Velocity, Microzonation, Site response

This research did not receive any specific grant from funding agencies in the public, commercial, or not-for-profit sectors.

1.0 Introduction

Anchorage (USA) is home to approximately half the State of Alaska's population (approximately 300,000 people) and is located in a highly active tectonic setting. Anchorage was devastated by the 1964 Great Alaska Earthquake, which is the world's second-largest earthquake in recorded history, with a moment magnitude (M_W) of 9.2 [1]. More recently, an M_W7.1 earthquake struck southcentral Alaska in November 2018, resulting in damage throughout the region, including Anchorage [2]. As shown in Fig. 1, seismicity around Anchorage is attributed to earthquakes originating from several sources including interface and intraslab events [3] related to the subducting Pacific plate diving below the North American plate at a rate of 55mm/yr [4]. There are also several crustal faults within the region [5].

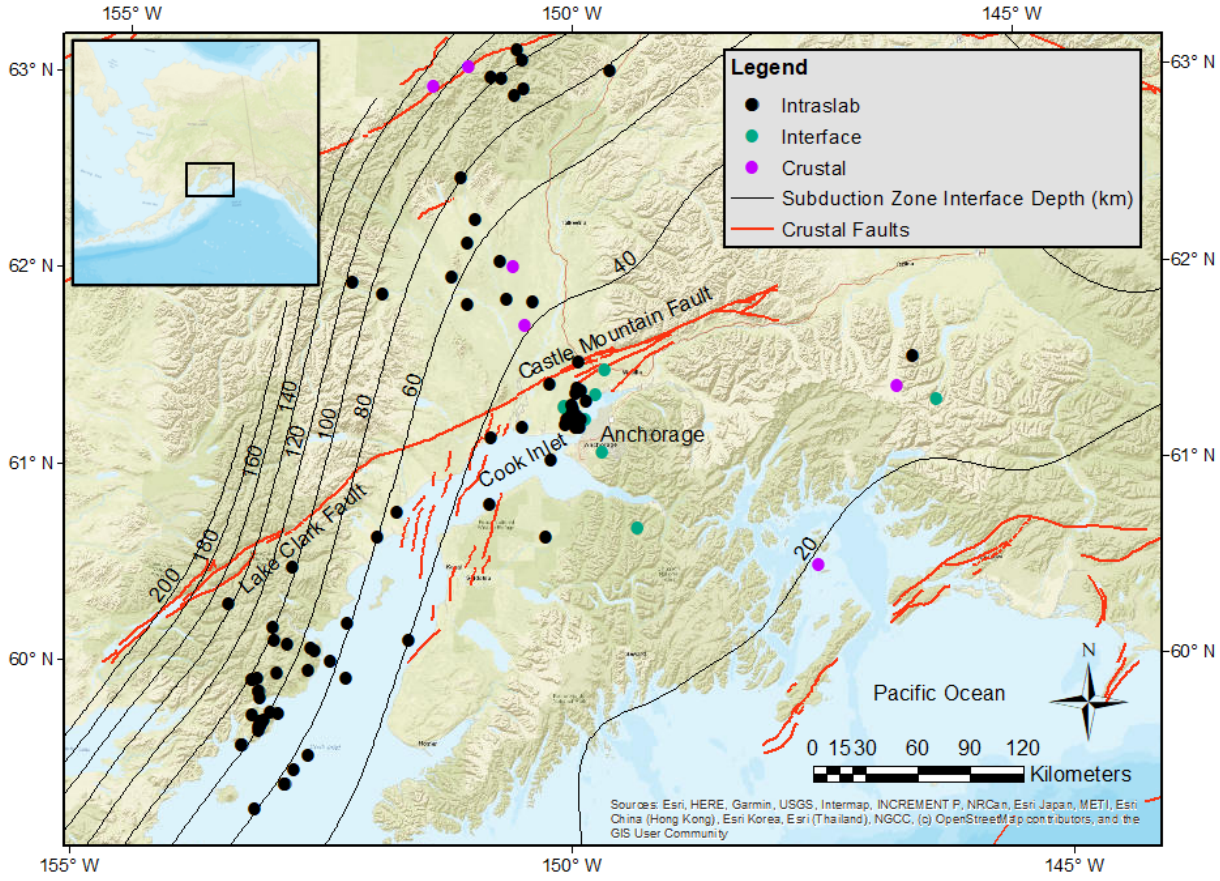

Fig. 1 Southcentral Alaska's tectonic setting. The contours indicate the depth of the interface between the subducting Pacific plate and the North American plate and regional crustal faults [5]. The earthquake epicentral locations used in this study are shown as circles and have been further divided into intraslab, interface, and crustal events. The inset figure indicates the location in Alaska considered for this study.

Due to frequent earthquakes in the region, numerous strong-motion sensors have been installed in and around Anchorage to better assess ground motion characteristics in the area. Thornley et al. [6] have utilized recent recordings from 35 strong-motion stations to evaluate the variability of spectral amplification across Anchorage, using standard spectral ratio (SSR) techniques, defined as Fourier amplitude spectral ratio between each site and a reference site. While analyses using SSR data are

useful for site response studies, other methods have also been found to offer efficiencies. A tool that has been found to be effective in estimating site response [7,8], especially in determining a site's fundamental frequency of vibration, is the horizontal to vertical spectral ratio (HVSR), where the horizontal ground response from an earthquake ground motion is divided by the vertical response at frequencies of interest.

HVSR analysis is useful in several ways. The results can be used to interpret the soil layering from a velocity perspective [e.g., 9,10,11], and the results can provide the fundamental frequency of a site [e.g., 12,13]. HVSR has also been used to estimate the time-averaged shear-wave velocity in the upper 30m (V_{S30}) of a site for engineering applications. For example, the NEHRP site classifications have recently been divided into eight new groups based on V_{S30} [14], which adds three categories to the previous classification system. These classifications are used to calculate the site amplification based on V_{S30} in building standards and codes throughout the United States. *Table 1* provides the V_{S30} ranges for each of the seismic site classes based on the changes to Table 20.3-1 of the 2020 NEHRP recommendations.

Table 1 Seismic Site Classification (modified from BSSC [14])

Site Class	**V_{S30} range (m/s)**
A: Hard rock	> 1,500
B: Rock	915 to 1,500
BC: Soft rock	640 to 915
C: Very dense soil and soft rock	440 to 640
CD: Very stiff soil	300 to 440
D: Stiff soil	215 to 300
DE: Soft soil	150 to 215
E: Soft clay soil	< 150

The HVSR are often easier to compute than SSR data because HVSR results do not require a reference-rock site. Therefore, the technique has been adopted widely when carrying out microtremor analysis using surface waves for site characterization in less active tectonic regions. However, it is noted that HVSR data used in this study were calculated using the S-wave portion of the earthquake records (rather than microtremors) collected at 35 strong-motion stations in Anchorage.

Studies by Nath et al [15], Dutta et al. [16], Biswas et al. [17], Thornley et al. [18], and others have utilized a variety of methods to estimate seismic characterization of several sites in the Anchorage basin. Nevertheless, there are still numerous strong-motion station sites in the Anchorage area where deep subsurface information is not available. These studies rely on methods to characterize Anchorage sites using shear-wave velocity, which is a fundamental property of the soil [19]. While V_{S30} is not a physical characteristic of site response [20], it is a common term used in ground motion prediction equations such as NGA-West2 [21] and NGA-Subduction [22], and code-based site characterization [23]. However, many have cautioned against the use of V_{S30} to describe deep soil deposits (e.g., [24]). The western portion of Anchorage consists of deeper soil deposits, and in some cases soil deposits that have low shear-wave velocities below 30m depth. Thornley et al. [18] have shown shear-wave velocities less than 300 m/s deeper than 40m at one site, where the profiling extended below 30m. Considering these deeper deposits were shown to be more effective for site response analyses of this deep soil site in Anchorage. Other areas in Anchorage are likely to fit a model based on an average of more than 30m.

The lack of available subsurface data requires consideration of various other methods including HSVR and SSR to estimate V_{S30}. This is necessary because of the adoption in Anchorage of the International Building Code, which classifies sites based on V_{S30}.

This article presents the results of the HVSR calculations for the strong-motion sites in Anchorage using a dataset from 2004-2019. Then the study provides a relationship between HVSR results and V_{S30} and its comparison to several studies from other parts of the world. A comparison of the HVSR and SSR results for the current dataset is also presented here. As a result of this analysis and the collection of other site-specific shear wave velocity data, a map showing the spatial distribution of V_{S30} in Anchorage is also presented.

2.0 Geology

Anchorage is bounded by the Cook Inlet (Pacific Ocean) on three sides with the Chugach Mountains rising at the eastern flank of the city. The Chugach Mountains, consisting of an accreted and lightly metamorphosed greywacke [25], dip steeply to the northwest. Anchorage has experienced several glacial episodes that have advanced and deposited various materials, from glacial outwash consisting of coarse sand and gravel to glaciolacustrine fine-grained silt and clay, which has created an area of complex geology. A simplified summary of the surficial geology is presented in Fig. 2a. Sedimentary soil thickness reaches a depth of 500m overlying bedrock at the city's western border [26,27,28]. The overlying deposits consist of a range of soils, from dense glacial till with shear-wave velocities greater than 1,000 m/s [18] to soft, cohesive lacustrine soil with shear wave velocities of 150 m/s [29]. Erosional events related to several glaciation events have affected the thickness and lateral deposition of these different soils [30,27]. The complex geology across Anchorage results in significant variability in ground shaking from earthquakes.

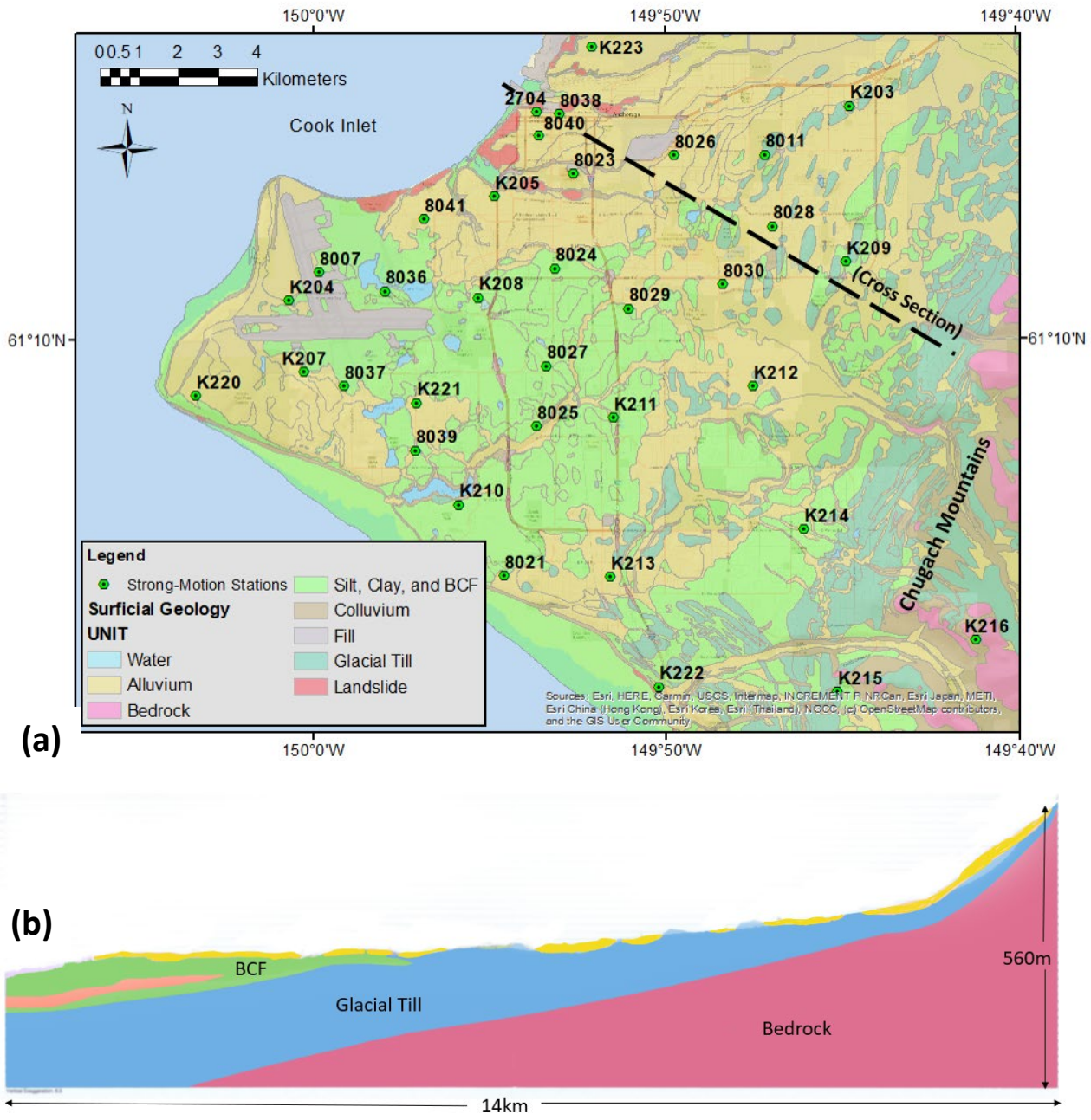

Fig. 2 Strong-motion station locations in Anchorage, Alaska. (a) The generalized surficial geology is provided in the background along with a cross-section location (dashed black line). Notably, the Bootlegger Cove Formation (BCF) is in green. (b) A simplified geologic cross-section depicting the variability of subsurface conditions across Anchorage (modified from Combellick [27]). Note the vertical exaggeration.

A layer of dense glacial till overlies the dipping bedrock across the city and is near the surface in the eastern portion of the city (Fig. 2b). Glacial till is overlain by glacial outwash in the northern part of the city. Overlying the glacial till in the central and western portions of the city are varying thicknesses of alluvium. The central soil unit has been found to have a significant impact on ground motions and site response is the Bootlegger Cove Formation (BCF). The BCF was deposited 10,000 to 14,000 years ago

over multiple glacial episodes in the region and has several facies of varying stiffness and makeup, including sand, silt, and clay [30]. One of the more sensitive clay facies was responsible for the 1964 Great Alaska Earthquake's significant ground failures. These failures included significant slope failures [31] and the formation of grabens [32]. A ground failure susceptibility map of the city, focused primarily on the anticipated effects of the BCF from future earthquakes, as published by Harding-Lawson Associates [33]. The BCF is generally centered in the city's middle portion with the more sensitive clay facies located in the north. The BCF is overlain by silt and sand in the south, depicted by fine-grained (silt and clay) and alluvial soil in Fig. 2a [29,27,34]. There is also some fill soil, such as in the western portion of the city at the Ted Stevens Anchorage International Airport, which is anthropogenic in nature.

3.0 Strong-Motion Stations and Dataset

Many strong-motion stations have been installed in south-central Alaska since the Great Alaska Earthquake in 1964. The current study utilizes strong-motion records of 95 earthquakes (locations shown in Fig. 1) measured at 35 stations across Anchorage (Fig. 2a). Appendix A provides the locations of the strong-motion stations and Appendix B provides the epicentral locations, depths, and magnitudes of the events used. The stations are primarily Kinemetrics force-balanced accelerometers with sampling rates of 200 Hz. The stations are set to record continuously. The stations are monitored by the Alaska Earthquake Center (AEC).

The dataset used in this study is described in considerable detail by Thornley et al. [6]. A total of 1,727 three-component recordings are used in the HVSR analysis. These records were collected between 2004 and 2019 and include the November 30, 2018, M_W7.1 Anchorage Earthquake. A large majority of the data was provided by AEC, with the Delaney Park Downhole Array (DPDA) data from the University of California, Santa Barbara (http://www.nees.ucsb.edu/), and some additional records from IRIS (https://www.iris.edu/hq/).

As mentioned in the introduction, there are three primary sources of earthquakes in the region. These include crustal, intraslab, and interface earthquakes, with the latter two being related to the subducting North American plate. The magnitude-epicentral distance relationship of the events used in this study is shown in Fig. 3. The time histories of the recorded data were pre-processed before the analysis. Initial processing was performed using Seismic Analysis Code (SAC) [35]. The records were filtered with a fourth-order Butterworth bandpass filter with corner frequencies of 0.1 and 30 Hz. Strong-motion records with a signal-to-noise ratio greater than three were used in this study. Anchorage is an urban center, and the building stock consists of buildings up to approximately 20 stories (fundamental frequencies around 0.5Hz). The frequencies of interest for the study were between 0.25 and 10 Hz, as that is a typical range for engineered infrastructure in Anchorage and the site effects at strong-motion stations utilized in this study have predominant frequencies within this range. In addition, the selected reference station is observed to have site amplifications above about 7Hz [36].

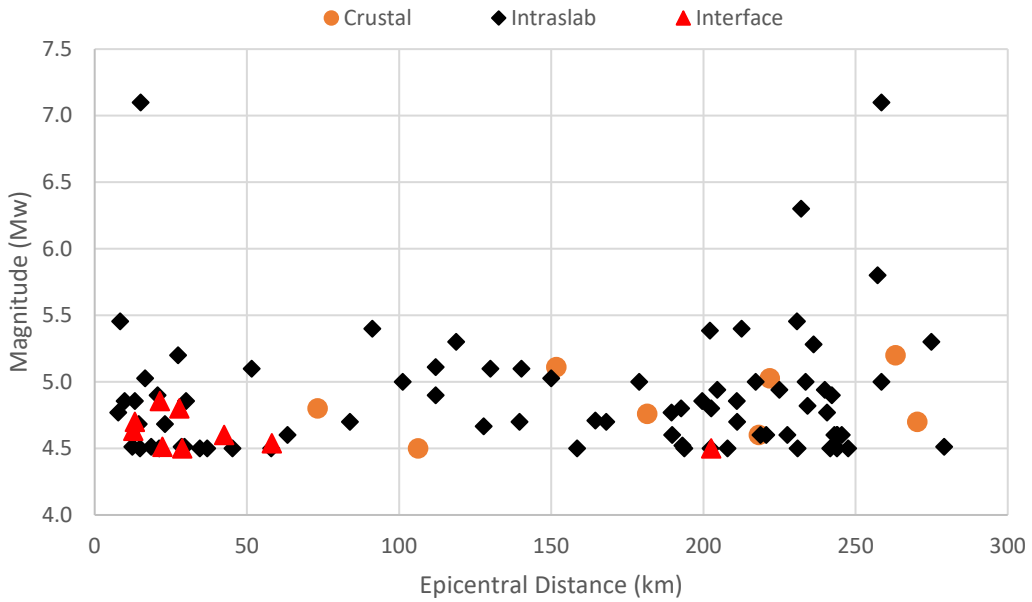

Fig. 3 Epicentral distances of the 95 events used in this study to central Anchorage versus magnitude with crustal, intraslab, and interface events identified. Distances are calculated from Station 8040 (Fig. 1) located in downtown Anchorage (location presented in Appendix A).

4.0 HVSR Analysis

The earthquake records selected for this study were analyzed using the GITANES program in MATLAB, which was developed by Klin [37]. The program utilizes the generalized inversion technique (GIT) to produce SSRs, where the stations are compared to a reference site. In this case, the reference site was the K216 rock site in southeast Anchorage (Fig. 1a). In addition to the SSR results, GITANES calculated the HVSR receiver function results from each station's input earthquake time histories. In Thornley et al. [6], the GIT approach is used to evaluate the variability of site response at 1 Hz and 5 Hz across Anchorage. In that study, little attention is paid to the ability of SSR to evaluate site response through estimates of V_{S30}.

In GITANES, the logarithmic mean of the Fourier amplitude spectra (FAS) of the two horizontal components is divided by the FAS of the vertical component for each frequency of interest. This method is preferred to the pseudo-spectral acceleration ratio method by Zhu et al. [13] because it avoids potential bias at sites with multiple peaks. The standard error is also calculated when several time histories are included for a station. In this study, the HVSR was calculated for each station over the 0.25 to 10 Hz frequency range, which provides for the fundamental frequencies of buildings and infrastructure typical in Anchorage. The HVSR results for each station are presented in Appendix C.

Because HVSR and SSR data provide overlapping information regarding a site, including the fundamental frequency and insight into site amplification, a comparison of the two datasets is presented in this study. It should be noted that HVSR data can be used to estimate the frequencies where site amplification occurs, but in many cases, there is no clear indication of the amplitude of the ground amplification [7], which is why SSR results derived from GIT or other means are often preferred.

The use of HVSR starts with the selection of the frequency where the peak amplification occurs, identified as f_{peak} throughout this study. Another term that is of importance is A_{peak}, defined as the amplitude corresponding to f_{peak}. Often this is recognized as the first peak [24] but has also been identified as the point where the highest peak is observed [34], which may not be the first peak. The following three examples demonstrate the situations that may lead to different peaks being selected. In the case of Fig. 4a, there is a clear peak, while in Fig. 4b the highest peak is not the first peak. The third case is where there is no clear highest peak, as shown in Fig. 4c. Studies including Zhu et al. [13] have evaluated the selection of peaks and found the highest peak is preferred to the first peak in characterizing site resonant frequencies. In this study, the highest peak is selected and used as f_{peak}.

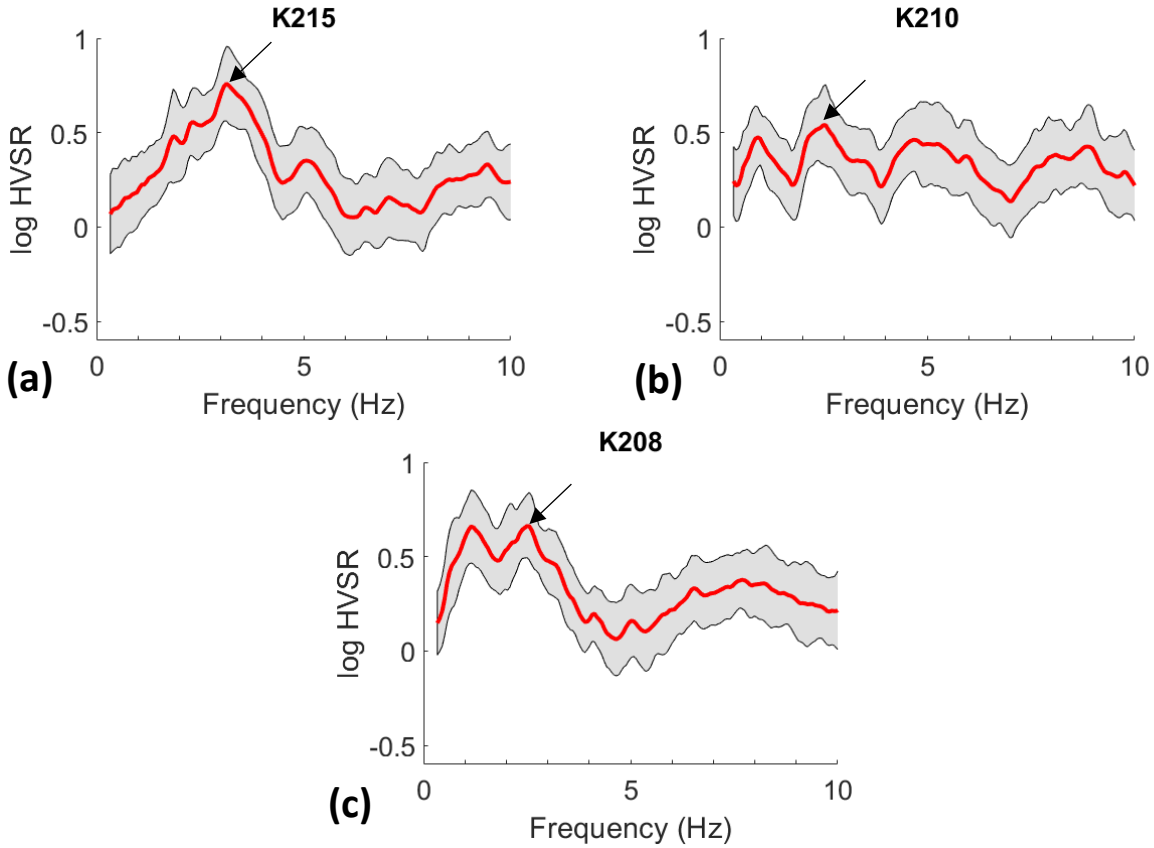

Fig. 4 HVSR data presenting three conditions where the selected peak may vary. (a) shows a single peak where the peak frequency is approximately 3Hz. (b) shows multiple peaks where the second peak is the highest peak. (c) shows double peaks where there are two peaks, and the amplitude of the highest peak is not much different from the amplitude of the second peak. Arrows indicate selected peaks.

5.0 Evaluation of V_{S30} by HVSR (an evaluation of several methods)

One of the main challenges with the Anchorage strong-motion network is the lack of subsurface characterization at many recording sites. Few sites have geotechnical data deeper than 10m, either at the site or nearby. This lack of information supports the need for studies like this to better estimate site characteristics and better understand the observed site response in Anchorage.

The V_{S30} for several strong-motion sites in Anchorage has been measured. Of the 35 stations evaluated in this study, 16 stations have an estimate of V_{S30}, 15 include surface measurements and only one has a

downhole V_S profile. In Dutta et al. [39] 15 strong-motion sites that are included in this study were evaluated using Rayleigh waves from an electromagnetic vibrator and V_{S30} was estimated. As mentioned previously, Thornley et al. [18] performed downhole testing at the DPDA to measure the time-averaged shear-wave velocity profile to a depth of 60m below ground surface. The V_{S30} measurements for these stations are included in Appendix A.

The use of f_{peak} from HVSR data to estimate V_{S30} for a site has been proposed in several studies, including regional studies using data from NGA-West2 and Japan [24], central and eastern portions of the United States (CEUS) by Hassani and Atkinson [38], and the study by Yaghmaei-Sabegh and Hassani [40] identified throughout this paper as the "Iran" study, among others. The study presented by Hassani and Atkinson [34] is focused on the CEUS where soft soils overlay hard bedrock. The eastern portion of Anchorage has some similarities to CEUS sites, where the loose sand and gravel overlies dense glacial till which can have shear-wave velocities greater than 1,000 m/s [18]. Because the V_S of these geologic units is greater than 760 m/s it is considered to be engineering bedrock from a shear-wave velocity perspective [23] . Fig. 5 presents the above-referenced models comparing f_{peak} from the HVSR data to measured V_{S30} for the stations shown in Appendix A.

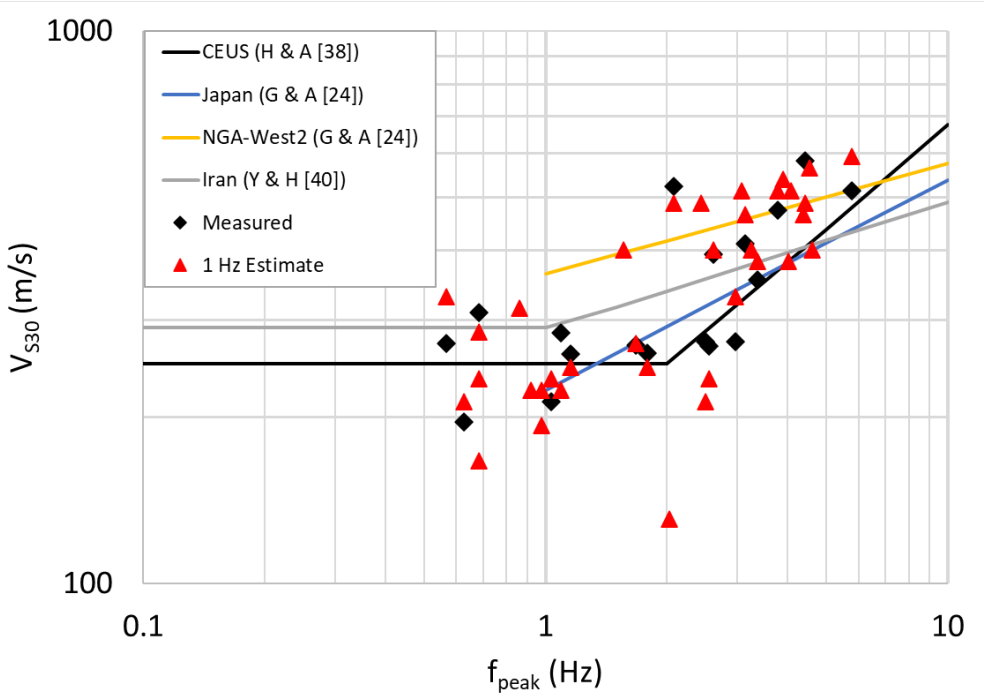

Fig. 5 V_{S30} data for several strong-motion stations in Anchorage and the HVSR f_{peaks} for those sites plotted with models from four different studies. The black diamonds represent measured V_{S30} data and the red triangles ("1 Hz Estimate") represent the results from an SSR estimate of V_{S30} (introduced subsequently). NGA-West2 and Japan models are only applicable from 1 to 10 Hz.

Locally, Dutta et al. [41] created a relationship between the SSR at 1 Hz and V_{S30}. To evaluate this relationship for the current dataset the logarithmic band-averaged SSR results for 1 Hz from Thornley et al. [6] have been used. The SSR results were calculated using the Fourier amplitude spectral ratios at each station with respect to the reference station, which is consistent with Dutta et al. [41]. The

logarithmic band-averaged results cover the 0.5 to 2.5 Hz frequency range of HVSR and SSR. It is observed that both studies yield similar results with independent datasets (Fig. 6).

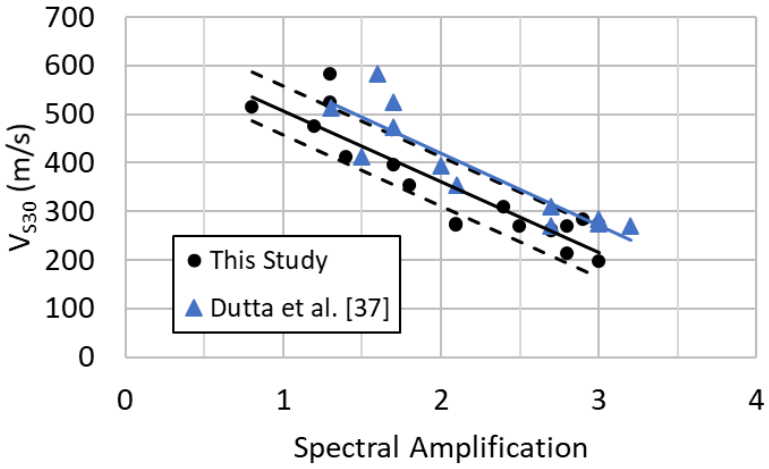

Fig. 6 Plot of the relationship between 1 Hz logarithmic band-averaged spectral amplification and measured V_{S30} profiles. The SSR values plotted for this study are from the results presented in Thornley et al. [6]. The dashed black lines present ±1 standard deviation for the data used in this study.

The relationship between V_{S30} and SSR at 1Hz is shown in the following equation obtained using least-squares repression:

$$V_{S30} = -145.9\ (\pm 17.1)(SSR_{1Hz}) + 652.9\ (\pm 38.4) \qquad \text{(Equation 1)}$$

where SSR_{1Hz} is the spectral amplification of the logarithmic band average about 1Hz. The model standard deviation is 50.4.

The 1 Hz band-averaged range is lower than the f_{peak} for the stiffer sites (Appendix A). In Anchorage, the sites with higher shear-wave velocity are located on the east side of the city and have estimated depths to engineering bedrock of less than 30m (Combellick [27]). When comparing the SSR results presented by Thornley et al. [6] and HVSR results, it is observed that the amplitudes across the frequencies of interest tend to overlap more for sites in central and western Anchorage (Fig. 7). A comparison of the HVSR and SSR plots for each station is included in Appendix C. For sites in the eastern portion of the city, where the depth to engineering bedrock is shallower, the frequency peaks are generally well aligned between the SSR and HVSR data. Still, the amplitudes of the HVSR curves tend to be higher within most of the 0.25 to 10 Hz range. SSR peak amplitudes range from 8% higher to 99% lower than A_{peak} values with an average of 25% lower (standard deviation of 29%). The stiffer sites such as K212 and K214 appear to have higher SSR peak amplitudes while the softer sites appear to have higher A_{peak} values.

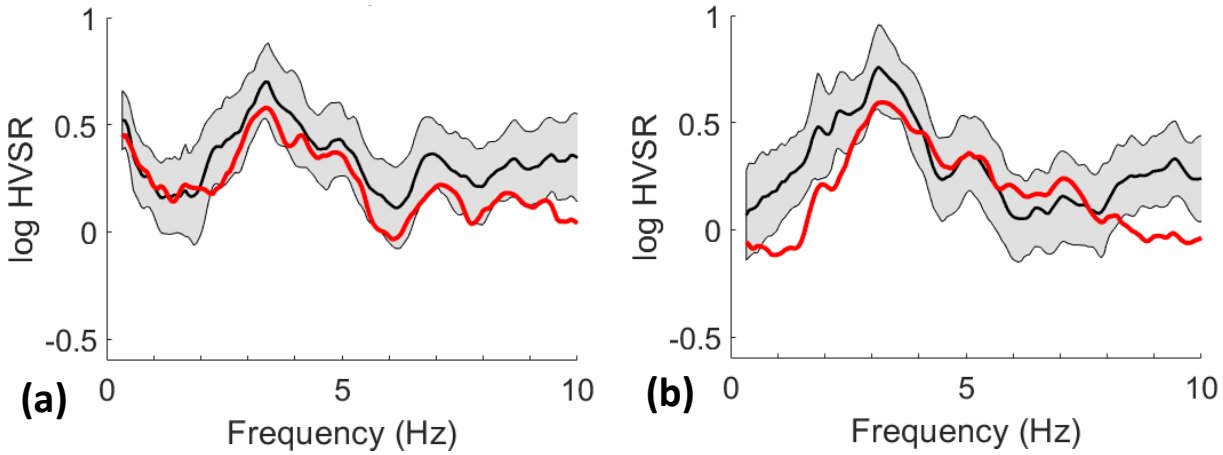

Fig. 7 HVSR (black line and grey shaded area is standard error range) and SSR (red line) plots of a station in (a) central Anchorage (K213) and (b) a site in eastern Anchorage (K215).

To further evaluate the relationship between HVSR and SSR the logarithmic band-averaged 1 Hz (0.5 to 2.5 Hz) and 5 Hz (4 to 6.5 Hz) values have been calculated and compared. The comparison utilizes a Bland-Altman difference plot [42] where the x-axis is the average of the two models and y-axis is the difference between the two models as summarized by the following relationship:

$$M(x,y) = \left(\frac{M_1+M_2}{2}, M_1 - M_2\right) \quad \text{(Equation 2)}$$

where M_1 and M_2 are the HVSR and SSR band-averaged values, respectively, for the frequencies of interest. Fig. 8 presents the plots of the function *M(x,y)* for two different frequencies (1 and 5 Hz) color-coded for corresponding V_{S30} ranges presented in Table 1. Points that plot closer to zero on the y-axis indicate a better fit between models. The median and ± one standard deviation values for the full dataset are included. In general, the sites with V_{S30} of less than 300 m/s appear to lead to a better fit between models for both 1 Hz and 5 Hz band-averages.

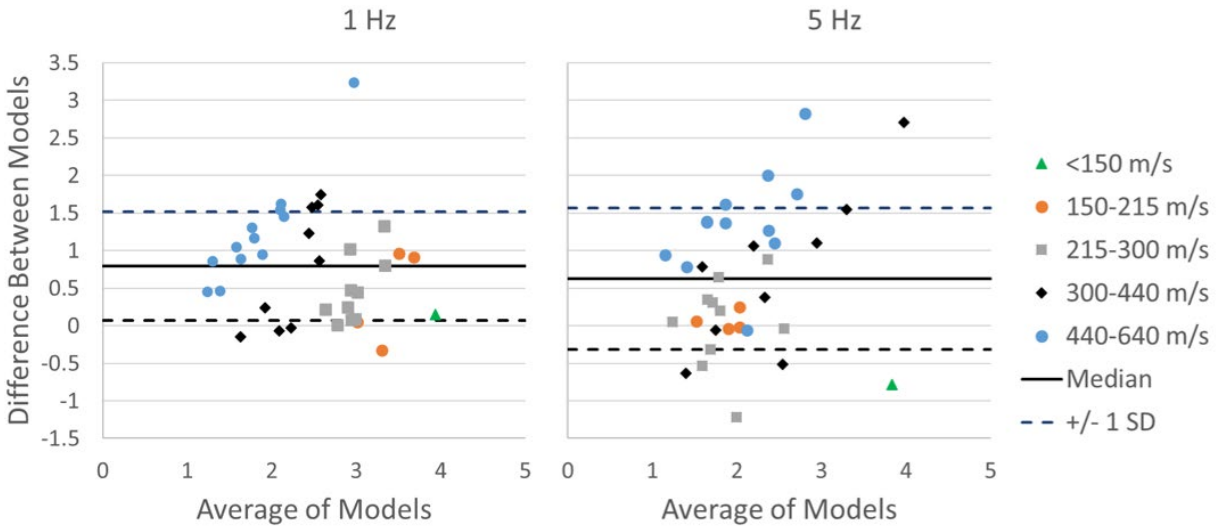

Fig. 8 Comparison between band-averaged SSR and band-averaged HVSR data at 1 and 5 Hz using a Bland-Altman difference plot for Anchorage data for the 35 stations in this study. The median and ± one standard deviation range of the dataset are shown as solid and dashed lines, respectively.

6.0 Relationship Between V_{S30} and HVSR

As noted above, several models may be used to estimate V_{S30} at strong-motion sites using either SSR or HVSR from earthquake records. The HVSR-based V_{S30} models by others presented in Fig. 5 show significant variability. These models have been developed from independent datasets for different tectonic regions. The CEUS model is for a relatively quiet tectonic region of the United States [39], particularly when compared to south-central Alaska. As noted previously, some similarities related to soil depth over stiffer material make the CEUS model useful in eastern Anchorage where the V_{S30} estimates are higher. Visual inspection of Fig. 5 suggests that the slope of the CEUS model at f_{peak} frequencies greater than 2 Hz tends to match the Anchorage data better than the other three models. To select the most appropriate model for estimating V_{S30} using HVSR data at strong-motion stations in Anchorage, a comparison is performed between the HSVR-based models (shown graphically in Fig. 5) and the band-averaged SSR model (Fig. 6). Fig. 9 presents the comparisons between the SSR model presented in Fig. 5 (red triangles) and the CEUS, Iran, Japan, and NGA-West2 models. A Bland-Altman difference plot described in Equation 2 is used to explore the differences.

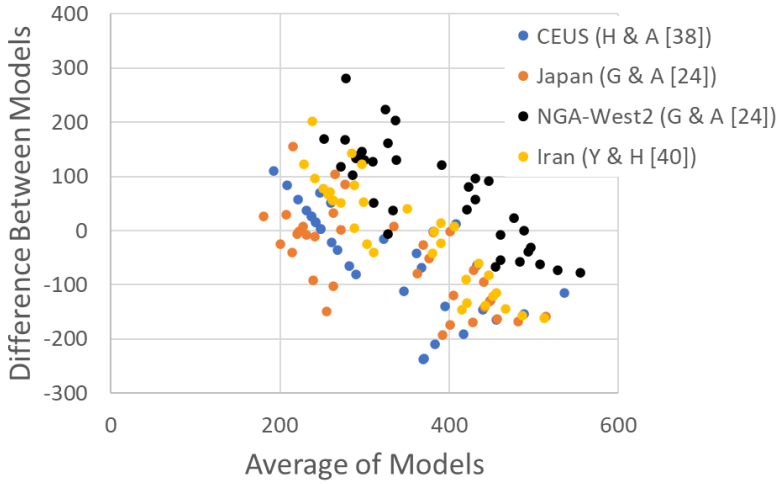

Fig. 9 Comparison of V_{S30} results for the 1 Hz band-averaged SSR and four HVSR-based models. (a) CEUS model, (b) Iran model, (c) Japan model, and (d) NGA-West2 model.

Several observations for Anchorage can be made based on the results presented in Fig. 9. The CEUS and Japan models tend to underpredict V_{S30} when compared to the 1 Hz band-averaged SSR model. The Iran model tends to overpredict lower V_{S30} values, which is partially a function of the lower bound of the model set to 290 m/s for f_{peaks} less than 1 Hz. The Iran model also tends to underpredict higher V_{S30} values. While the NGA-West2 model matches higher V_{S30} values more closely, there is a general overprediction of lower V_{S30} values than the 1 Hz band-averaged SSR model. These observations suggest that the other regional models considered are not as effective as the SSR model for estimating V_{S30} in Anchorage.

7.0 Comparison of f_{peak} and A_{peak} V_{S30} relationships to global models

Ghofrani and Atkinson [24] present a relationship between V_{S30} and f_{peak}. In that study, there was also a relationship presented between the peak amplitude of the H/V data and V_{S30}. While the Anchorage V_{S30} data at strong-motion stations are limited, the V_{S30} estimates developed from the 1 Hz SSR estimates can

be used in conjunction with the f_{peak} and A_{peak} HVSR results to further evaluate the appropriateness of the model when compared to global estimates.

In Ghofrani and Atkinson [24] the NGA-West2 dataset is used to develop the following equations:

$$\log(V_{S30}) = 0.20\log(f_{peak}) + 2.56 \text{ for } f_{peak} \geq 1Hz \quad \text{(Equation 3)}$$

and

$$\log(V_{S30}) = -0.46\log(A_{peak}) + 2.86 \quad \text{(Equation 4)}$$

with ± one standard deviation estimates of 0.16 and 0.15 log units for f_{peak} and A_{peak}, respectively. The V_{S30} estimates based on the 1 Hz spectral amplitude model, along with HVSR f_{peak} and A_{peak} results have been used to estimate local relationships between estimated V_{S30} and the HVSR f_{peak} and A_{peak} values. Fig. 10 presents the Anchorage data and provides a comparison with the NGA-West2 dataset. The relationship developed in the NGA-West2 study had a lower bound for f_{peak} of 1 Hz. The current study utilizes data below 1 Hz because there is no strong indication that 1 Hz was the appropriate cutoff.

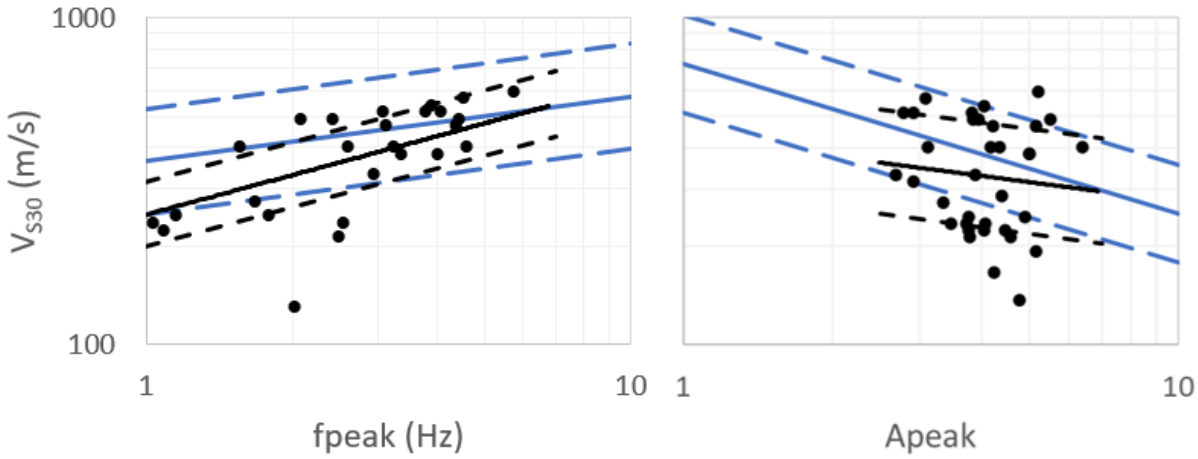

Fig. 10 Estimated V_{S30} relationship with HVSR f_{peak} and A_{peak} results, black circles. The regression line (solid black line with ± one standard deviation in black dashed lines) shows that the results generally fit

within the median ± one standard deviation (blue solid and dashed lines, respectively) for the NGA-West2 dataset, as presented in Fig. 8 of Ghofrani and Atkinson [24].

The resulting equations (Equations 5 and 6) have been developed to describe the estimated V_{S30} for Anchorage from HVSR f_{peak} and A_{peak} values:

$$\log(V_{S30}) = (0.40 \pm 0.03)\log(f_{peak}) + (2.40 \pm 0.09) \qquad \text{(Equation 5)}$$

and

$$\log(V_{S30}) = -(0.20 \pm 0.08)\log(A_{peak}) + (2.64 \pm 0.3) \qquad \text{(Equation 6)}$$

When Equations 5 and 6 are combined, the following relationship is developed to estimate V_{S30} with both f_{peak} and A_{peak}:

$$\log(V_{S30}) = (0.37 \pm 0.04)\log(f_{peak}) - (0.36 \pm 0.1)\log(A_{peak}) + (2.72 \pm 0.2) \qquad \text{(Equation 7)}$$

The standard deviations for Equations 5 through 7 are 0.10, 0.16, and 0.09 log units, respectively. Equations 5 and 7 are only valid for values of $f_{peak} \geq 1$ Hz. The results of the relationship between the estimated V_{S30} and HVSR values for f_{peak} and A_{peak} are generally similar to the NGA-West2 dataset, especially at higher V_{S30}. However, the slope of f_{peak} with V_{S30} is steeper than the NGA-West2 slope. This result agrees well with the visual observation that can be made in Fig. 5. While it does not appear to be particularly strong due to the wide spread of data points, the relationship with A_{peak} is similar to the NGA-West2 dataset but with the slope of the current dataset being flatter than the NGA-West2 trend. These results suggest that as the V_{S30} increases, the f_{peak} increases at a higher rate indicating that the underlying glacial till in the eastern portion of Anchorage has a high shear-wave velocity, which is in better agreement with the CEUS model presented in Fig. 5. However, the shallow slope of the trendline of the A_{peak} relationship suggests that the amplitude of the HVSR results does not reduce as quickly, indicating that A_{peak} may not be as sensitive an indicator of V_{S30} in Anchorage as it is in other regions.

8.0 V_{S30} Map of Anchorage

The subsurface geology of Anchorage is complex and varies significantly, especially from east to west. One indicator of this variability is V_{S30} at the strong-motion stations, which represent 35 locations where V_{S30} can be estimated, based on the models presented above. In addition to these data points, we have also collected V_{S30} estimates from public and private projects across Anchorage to provide a higher density of data points. The private projects represent a large collection of downhole V_{S30} estimates, which are presented as black triangles in Fig. 10, but are not publicly available, except for Thornley et al. [18]. Additionally, Dutta et al. [39] performed V_{S30} assessments at several additional locations that were collocated with current and previous strong-motion stations and other selected locations. These data were not used in the development of the correlations above because the strong-motion stations had been dismantled did not record events used in this study. The compilation of these data provides more than 70 discrete locations where V_{S30} has been estimated in Anchorage. A contour map showing the variability of V_{S30} across Anchorage is presented in Fig. 11. The V_{S30} values used at the strong-motion stations have been calculated utilizing the SSR relationship illustrated in Fig. 6 and are included in Appendix A. Additional sites presented by Dutta et al. [39] are provided in Appendix D. When comparing this map to that of Dutta et al. [41] there is a general trend moving from east to west that is the same on both maps. However, with an additional 34 locations where V_{S30} has been estimated,

additional granularity is developed by the newer map. This is especially evident in areas where V_{S30} estimates are less than 215m/s, which agree with the local geologic conditions, and are discussed further below.

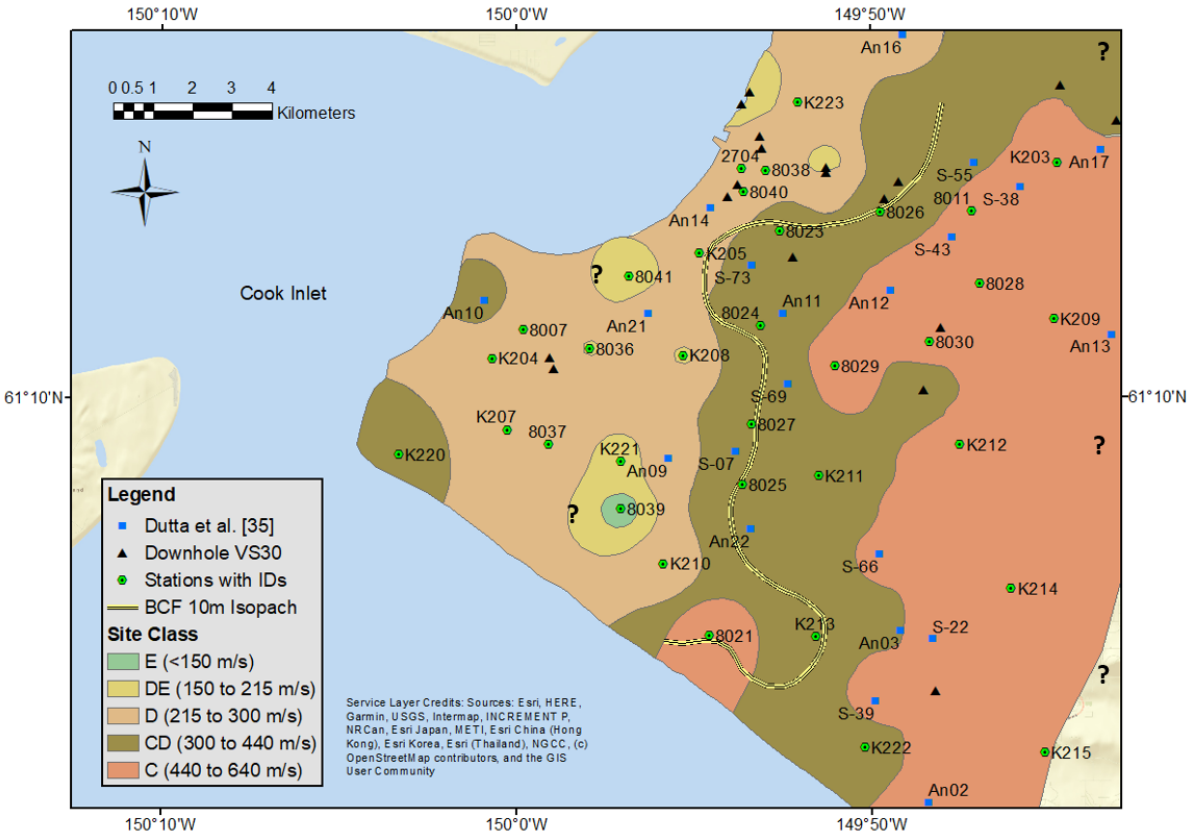

Fig. 11 Contour map of BSSC [14] Seismic Site Class, based on V_{S30} estimates at strong-motion stations and measurements at other locations across Anchorage.

The contour lines used for Fig. 11 have been calculated utilizing the inverse distance weighting to a power gridding method in Surfer (version 17.1.288) from Golden Software, LLC (goldensoftware.com) with a power exponent of three and no smoothing. The site classes are those in the revised seismic site classifications presented in the 2020 National Earthquake Hazard Reduction Program (NEHRP) guidelines by BSSC [14]. Site classes have been color-coded in Fig. 11, identifying areas expected to have similar V_{S30}. This contour map may be useful for planning within Anchorage and could be used as the first estimate of seismic site classification when planning geotechnical investigations. As expected, the stiffer soil with higher site classes is found on the east side of Anchorage. The interface between site class C soil and the stiffer BC and B sites (Table 1) to the east has not been estimated due to a lack of information other than surficial geology. Still, this area on the east side of Anchorage is much less inhabited and is typically reserved as parkland.

There is a clear area just west of the site class C zone that can be defined as a site class CD. This zone indicates a transition between the glacial tills to the east and the BCF soils in central and western Anchorage. Site class D regions agree well with regions of deeper BCF soil [30,29,27]. There are two zones of site class D/E in western Anchorage (i.e., at Stations 8039 and 8041). These areas are indicative

of deeper, and softer soil areas, as also described by Updike and Ulery [29]. In these two regions there are deeper pockets of BCF silts and clays. The results from this study suggest that deeper BCF deposits indicate a softer site class as well. At the western edge of Anchorage, the site class increases to site class CD, which is in general agreement with other studies showing that the western edge, despite having deep soil deposits, is generally stiffer than the middle portions of Anchorage. This area is also at the western fringe of the BCF, with only thin pockets of soft soil.

As mentioned previously, one of the assumptions for using f_{peak} as an indicator of V_{S30} is that the shear-wave velocity increases with depth. Station 8040, located in northern Anchorage, was found by Thornley et al. [18] to have BCF soil to depths greater than 40m with higher shear-wave velocity overlying zones of soil with lower shear-wave velocity and then increasing again. The estimates of V_{S30} and the measured V_{S30} show general agreement and the site is classified as a site class D in both cases. Strong-motion stations 8039 and 8041 indicate areas of lower V_{S30}, and it is possible that the surficial soil has a higher shear-wave velocity than the BCF deposits at depth, indicating that f_{peak} or SSR methods may not provide an adequate estimate of V_{S30} in these areas. Additional study at these sites is necessary to understand the impact of this potential velocity inversion on f_{peak} and other HVSR parameters. This may also be important for other areas in the city where deeper soil deposits, significantly deeper BCF deposits, are encountered. Figure 11 presents regions where similar shear wave velocity is estimated. There is likely to be additional variability, related to the geologic variability and the built environment that may shift or modify the site class boundaries. Further study will help define the lateral changes in V_{S30} across Anchorage. However, because V_{S30} is an important parameter in site response analysis for engineering design when using the building code, this map provides the most up-to-date estimate of the variability of V_{S30} across Anchorage. It should be noted that it does not attempt to identify sites where liquefaction may occur (i.e., site class F) so proper site characterization of the near surface is still required for future developments.

9.0 Concluding Remarks

Anchorage, Alaska, is situated in an active tectonic region experiencing both crustal and subduction earthquakes. Earthquake records from 35 strong-motion stations have been utilized to evaluate relationships between HVSR and site response, especially the site maximum peak frequency and its relationship to V_{S30}. Two regional relationships have been established including one between f_{peak}, A_{peak}, and V_{S30} and a second relationship between SSR and V_{S30} (Fig. 6), which can be utilized for future studies in the region.

In addition to the HVSR relationship, a V_{S30} contour map of Anchorage indicating estimated seismic site classes for all locations has been developed. This map can be utilized by planners and engineers as it can be used to provide first-order estimates of earthquake site amplification within Anchorage. There are areas within the confines of the map that lack data, such as the eastern edge where the site class boundary between site class C and site class BC has not been established, despite the likelihood of shallow bedrock. There are additional areas in western Anchorage where further study may validate the relationship between the geologic conditions and V_{S30}. As noted throughout the text, there are limitations with the use of V_{S30} to estimate site response. Further study is needed to evaluate methods that may be more dependable for site response characterization in deeper and more variable soil deposits.

Acknowledgments

The authors would like to thank several individuals for their contributions to the information included in this study. Dave Cole (retired DOWL), Keri Nutter (DOWL), Buzz Scher (retired R&M), and Dave Hemstreet (Alaska Department of Transportation and Public Facilities) provided shear-wave velocity profiles and other data used in the V_{S30} map. Andy Garrigus (Golder Associates) supported the development of the V_{S30} contour map. Drs. Natalia Ruppert and Mike West, along with Mitch Robinson (all with AEC) provided data and support. We thank Dr. Behzad Hassani and an anonymous reviewer for their detailed comments on an earlier version of this article.

References

[1] USGS.gov, 2020, https://earthquake.usgs.gov/earthquakes/events/alaska1964/, last accessed May 30, 2020.

[2] West, M. E., A. Bender, M. Gardine, L. Gardine, K. Gately, P. Haeussler, W. Hassan, et al., 2020, The 30 November 2018 Mw 7.1 Anchorage Earthquake. *Seismological Research Letters*, 91(1), 66–84. DOI: 10.1785/0220190176

[3] Wesson, R.L., O.S. Boyd, C.S. Mueller, C.G. Bufe, A.D. Frankel, M.D. Petersen, 2007, Revision of time-Independent probabilistic seismic hazard maps for Alaska: U.S. Geological Survey Open-File Report 2007-1043.

[4] Haeussler, P. J. 2008. An overview of the neotectonics of interior Alaska: Far-field deformation from the Yakutat microplate collision, in Active Tectonics and Seismic Potential in Alaska, J. T. Freymueller, P. J. Haeussler, R. Wesson, and G. Ekström (Editors), Geophysics Monograph Series, Vol. 179, American Geophysical Union, Washington, D.C., 83–108, doi: 10.1029/179GM05.

[5] Koehler, R.D., R.E. Farrell, P.A.C. Burns, and R.A. Combellick,, 2012, Quaternary faults and folds in Alaska: A digital database, in Koehler, R.D., Quaternary Faults and Folds (QFF): Alaska Division of Geological & Geophysical Surveys Miscellaneous Publication 141, 31 p., 1 sheet, scale 1:3,700,000. http://doi.org/10.14509/23944.

[6] Thornley, J., J. Douglas, U. Dutta, Z. Yang., 2021, Site Response Analysis of Anchorage, Alaska Using Generalized Inversions of Strong-Motion Data (2014-2019), Geophysical Journal International (In Review).

[7] Field, E.H., and K.H. Jacob, 1995, A Comparison and Test of Various Site-Response Estimation Techniques, Including Three that are not Reference-Site Dependent, Bulletin of the Seismological Society of America, 85, 1127-1143.

[8] Bonilla, F.L., Steidl, J.H., Lindley, G.T., Tumarkin, A.G. and Archuleta, R.J., 1997, Site amplification in the San Fernando Valley, CA: variability of site effect estimation using the S-wave, coda and H/V methods, Bulletin of the Seismological Society of America. 87, 710-730.

[9] Ibs-von Seht, M. and J. Wohlenberg, 1999, Microtremor Measurements Used to Map Thickness of Soft Sediments, Bulletin of the Seismological Society of America 89, 250-259.

[10] Castellaro S., F. Mulargia, 2009, VS30 estimates using constrained H/V measurements. Bulletin of the Seismological Society of America 99:761–773. https ://doi.org/10.1785/01200 80179

[11] Mundepi, A.K., C. Lindholm, and Kamal, 2009, Soft Soil Mapping Using Horizontal to Vertical Spectral Ratio (HVSR) for Seismic Hazard Assessment of Chandigarh City in Himalayan Foothills, North India, Journal Geological Society of India, Vol. 74, November 2009, pp. 551-558.

[12] Parolai, S. and S. Richwalski, 2004, The importance of Converted Waves in Comparing H/V and RSM Site Response Estimates, Bulletin of the Seismological Society of America, Vol. 94, No. 1, pp 304-313, 2004.

[13] Zhu, C., F. Cotton, and M. Pilz, 2020, Detecting Site Resonant Frequency Using HVSR: Fourier versus Response Spectrum and the First versus the Highest Peak Frequency, *Bulletin of the Seismological Society of America* 110, 427–440, doi: 10.1785/0120190186

[14] Building Sciences Safety Council (BSSC), 2019, BSSC Project Final Report: Development of the Next Generation of Seismic Design Value Maps for the 2020 NEHRP Provisions, National Institute of Building Sciences.

[15] Nath S.K., D. Chatterjee, N.N. Biswas, M. Dravinski, D.A. Cole, A. Papageorgiou, J.A. Rodriguez, and C.J. Poran, 1997, Correlation Study of Shear Wave Velocity in Near Surface Geological Formations in Anchorage, Alaska, Earthquake Spectra, Vol. 13, No. 1, February 1997.

[16] Dutta, U., A. Martirosyan, N. Biswas, A. Papageorgiou, R. Combellick, 2001, Estimation of S-Wave Site Response in Anchorage, Alaska, from Weak-Motion Data Using Generalized Inversion Method, Bulletin of the Seismological Society of America, 91, 2, pp. 335-346, April 2001.

[17] Biswas, N., A. Martirosyan, U. Dutta, A. Papageorgiou, and R. Combellick, 2003, *Seismic Microzonation: Metropolitan area of Anchorage*. Part A and B. Final Report prepared for Alaska Science and Technology Foundation, Geophysical Institute, University of Alaska Fairbanks, Fairbanks, AK.

[18] Thornley, J., Dutta, U., Fahringer, P., Yang, Z., 2019, In Situ Shear-Wave Velocity Measurements at the Delaney Park Downhole Array, Anchorage, Alaska. *Seismological Research Letters*, Volume 90, Number 1, January/February 2019 (p 395-400).

[19] Hashash, Y. 2014, 2014 Ralph B. Peck Lecture: Innovations in Modeling and Monitoring Technology for Response of Deep Urban Excavations, American Society of Civil Engineers Geo-Congress, Atlanta, GA, 2014.

[20] Idriss, I. M., (2011). Use of Vs30 to represent local site conditions, in 4th LASPEI/IAEE International Symposium Effects of Surface Geology on Strong Ground Motions, Santa Barbara, CA.

[21] Boore, D., J. Stewart, E. Seyhan, G. Atkinson, 2013, NGA-West2 Equations for Predicting Response Spectral Accelerations for Shallow Crustal Earthquakes, Pacific Earthquake Engineering Research Center Report 2013/05.

[22] Bozorgnia, Y., 2020, Data Resources for NGA-Subduction Project, Pacific Earthquake Engineering Research Center Report 2020/02.

[23] American Society of Civil Engineers (ASCE), 2017, *ASCE/SEI 7-16 Minimum Design Loads and Associated Criteria for Buildings and Other Structures*, American Society of Civil Engineers.

[24] Ghofrani H., G.M. Atkinson, (2014), Site condition evaluation using horizontal-to-vertical response spectral ratios of earthquakes in the NGA-West 2 and Japanese databases. Soil Dynamics and Earthquake Engineering, Vol. 67, 2014.

[25] Wilson, F. H.; C.P. Hults, H.R. Schmoll, P.J. Haeussler, 2012, Geologic map of the Cook Inlet region, Alaska, including parts of the Talkeetna, Talkeetna Mountains, Tyonek, Anchorage, Lake Clark, Kenai, Seward, Iliamna, Seldovia, Mount Katmai, and Afognak 1:250,000-scale quadrangles. Reston, VA, p. i-71. 2012. (3153).

[26] Glass, R.L., 1988, Map Showing Depth to Bedrock, Anchorage, Alaska. Open File Report 88-198, USGS. 1988. doi: 10.3133/ofr88198

[27] Combellick, R.A., 1999, Simplified geologic map and cross sections of central and east Anchorage, Alaska, Alaska Division of Geological & Geophysical Surveys Preliminary Interpretive Report 1999-1, 13 p., 2 sheets. http://doi.org/10.14509/2243.

[28] Schmoll, H.R. and W.W. Barnwell, 1984, East-west geologic cross section along the DeBarr Line, Anchorage, Alaska: U.S. Geological Survey Open-File Report 84-791, 10 p., 1 sheet.

[29] Updike, R.G. and C.A. Ulery, 1986, Engineering-Geologic Map of Southwest Anchorage, Alaska. Alaska Division of Geological and Geophysical Surveys Professional Report 89, sheet 1 of 1.

[30] Ulery, C.A., and R.G. Updike, 1983, Subsurface structure of the cohesive facies of the Bootlegger Cove formation, southwest Anchorage: Alaska Division of Geological & Geophysical Surveys Professional Report 84, 5 p., 3 sheets, scale 1:15,840. http://doi.org/10.14509/2257

[31] Hansen, W. R. 1965, Effects of the earthquake of March 27, 1964, at Anchorage, Alaska, U.S. Geological Survey Professional Paper (542-A), 68 pp.

[32] Shannon & Wilson, 1964, "Anchorage Area Soil Studies," U.S. Army Engineer District, Alaska, Corps of Engineers.

[33] Harding-Lawson Associates, 1979, "Seismically-Induced Ground Failure Susceptibility", Geotechnical Report for Municipality of Anchorage, Alaska.

[34] Schmoll, H.R. and E. Dobrovolny, 1972, Generalized geologic map of Anchorage and vicinity, Alaska. US Geologic Survey Misc. Geol. Invest. Map I-787-D.

[35] Goldstein, P., A. Snoke, 2005, "SAC Availability for the IRIS Community", Incorporated Institutions for Seismology Data Management Center Electronic Newsletter.

[36] Martirosyan, A., U. Dutta, N. Biswas, A. Papageorgiou, and R. Combellick (2002). Determination of site response in Anchorage, Alaska, on the basis of spectral ratio methods, *Earthquake Spectra* 18, 85–104.

[37] Klin, P., 2019, GITANES (https://www.mathworks.com/matlabcentral/fileexchange/61711-gitanes), MATLAB Central File Exchange. Retrieved August 2019.

[38] Hassani, B., G.M. Atkinson, (2016), Applicability of the Site Fundamental Frequency as a *VS*30 Proxy for Central and Eastern North America. *Bulletin of the Seismological Society of America*; 106 (2): 653–664. doi: https://doi.org/10.1785/0120150259

[39] Dutta, U., N. Biswas, A. Martirosyan, S. Nath, M. Dravinski, A. Papageorgiou, R. Combellick, 2000, Delineation of Spatial Variation of Shear Wave Velocity with High-Frequency Rayleigh Waves in Anchorage, Alaska, Geophysical Journal International (2000) 143, 365-375.

[40] Yaghmaei-Sabegh, S., B. Hassani, (2020), Investigation of the relation between Vs30 and site characteristics of Iran based on horizontal-to-vertical spectral ratios. Soil Dynamics and Earthquake Engineering, Vol. 128, January 2020, https://doi.org/10.1016/j.soildyn.2019.105899

[41] Dutta, U., N. Biswas, A. Martirosyan, A. Papageorgiou, S. Kinoshita, 2003, Estimation of Earthquake Source Parameters and Site Response in Anchorage, Alaska from Strong-Motion Network Data Using Generalized Inversion Method, *Physics of the Planetary Interiors*, 137 (2003) pp. 13-29. doi:10.1016/S0031-9201(03)00005-0

[42] Bland, J.M., and D.G. Altman, 1986, Statistical Methods for Assessing Agreement Between Two Methods of Clinical Measurement, Lancet 327 (8476): 307-10.

[43] Goulet, C., Y. Bozorgnia, N. Abrahamson, N. Kuehn, L. Al Atik, R. Youngs, R. Graves, G. Atkinson, 2018, Central and Eastern North America Ground-Motion Characterization, NGA-East Final Report, Pacific Earthquake Engineering Research Center, PEER Report No. 2018/08.

Appendix A: Station Locations and V_{S30} Estimates and the f_{peak} and A_{peak} results from the HVSR analysis.

Station Code	Latitude (°N)	Longitude (°W)	V_{S30} Estimate (m/s)	V_{S30} Measured (m/s)[1,2]	f_{peak} Hz	A_{peak}
K203	61.22007	149.7453	513	474[1]	3.78	3.82
K204	61.17581	150.0114	285	309[1]	0.68	4.40
K205	61.19963	149.9138	224	284[1]	1.09	4.47
K207	61.15957	150.0044	272	270[1]	1.68	3.35
K208	61.17646	149.9215	213	274[1]	2.50	4.59
K209	61.18455	149.7471	488	582[1]	4.42	3.85
K210	61.12923	149.9310	235	269[1]	2.55	3.47
K211	61.14905	149.8578	402	394[1]	2.61	4.18
K212	61.15622	149.7916	594	514[1]	5.77	5.22
K213	61.11262	149.8595	383	354[1]	3.37	5.01
K214	61.12353	149.7677	488	524[1]	2.09	5.51
K215	61.08625	149.7521	465	412[1]	3.14	5.15
K220	61.15404	150.0553	330		0.57	2.69
K221	61.15245	149.9510	193	277[1]	0.98	5.16
K222	61.08757	149.8366	315		0.86	2.92
K223	61.2338	149.8675	224		0.92	4.05
2704	61.21883	149.8940	224		0.98	3.77
8007	61.18236	149.9968	235		0.68	3.73
8011	61.20898	149.7857	513		3.08	2.79
8021	61.11293	149.9095	513	428[1]	4.07	2.91
8023	61.20469	149.8762	402		4.60	6.38
8024	61.18314	149.8853	402		3.26	4.36
8025	61.14716	149.8939	439		4.36	4.21
8026	61.20890	149.8289	383		4.01	5.01
8027	61.16087	149.8894	330		2.96	3.88
8028	61.19264	149.7823	565		4.54	3.08
8029	61.17392	149.8503	488	520[1]	2.43	3.94
8030	61.17949	149.8058	538		3.90	4.05
8036	61.17794	149.9657	213		0.62	3.79
8037	61.15625	149.9850	246		1.79	3.76
8038	61.21844	149.8829	235		1.03	4.06
8039	61.14162	149.9512	137		20.3	4.78
8040	61.21350	149.8930	264	264[2]	1.15	4.90
8041	61.19438	149.9471	167		0.68	4.23

Note: 1. Measurements from Dutta et al. [39]. 2. Measurement from Thornley et al. [18].

Appendix B: Earthquake Event Locations

Date (YYYY-MM-DD)	Latitude (°N)	Longitude (°W)	Depth (km)	Magnitude (M_W)
2005-02-16	61.326	149.853	35	4.6
2005-04-06	61.454	146.518	17	4.8
2005-04-17	60.771	149.311	27	4.5
2005-05-19	60.017	152.693	96	5.4
2005-08-15	60.130	152.675	103	4.5
2006-03-03	59.791	153.062	99	4.8
2006-03-17	60.706	152.024	81	4.7
2006-06-18	61.926	150.427	61	4.7
2006-07-27	61.155	149.678	36	4.7
2006-09-06	61.621	149.930	41	4.5
2007-09-19	61.375	146.105	31	4.5
2007-11-28	61.911	151.127	70	5.0
2008-03-27	59.010	152.169	69	5.3
2008-04-26	63.020	151.556	12	4.6
2008-09-18	59.503	152.793	90	4.5
2008-10-08	60.115	152.640	104	4.8
2008-10-12	63.161	150.553	123	4.6
2008-11-09	59.997	153.019	127	5.0
2008-11-29	63.111	149.577	95	4.7
2008-12-13	60.886	150.859	46	4.6
2008-12-28	62.346	151.055	89	4.7
2009-01-24	59.430	152.888	98	5.8
2009-02-15	61.603	146.334	37	4.5
2009-04-07	61.454	149.743	33	4.8
2009-04-10	63.495	151.737	14	4.7
2009-04-14	60.158	153.057	118	4.5
2009-04-30	58.993	151.311	53	5.0
2009-05-24	59.775	153.249	125	4.6
2009-06-22	61.939	150.704	65	5.4
2009-08-19	61.228	150.858	66	5.1
2010-04-07	61.580	149.652	35	4.6
2010-05-24	59.982	152.311	71	4.6
2010-07-08	61.805	150.505	15	4.8
2010-08-14	59.965	153.209	141	4.6
2010-09-15	59.861	153.176	121	5.0
2010-09-20	61.115	150.219	45	4.9

Date (YYYY-MM-DD)	Latitude (°N)	Longitude (°W)	Depth (km)	Magnitude (M_W)
2011-01-23	63.542	150.865	16	5.2
2011-02-04	60.725	150.276	41	4.5
2011-07-28	62.049	151.303	87	5.3
2013-01-13	60.541	152.904	134	5.0
2013-03-13	62.556	151.230	84	4.7
2013-08-01	60.145	152.918	126	4.8
2013-08-27	63.213	150.624	128	4.9
2014-03-12	59.296	153.177	86	4.5
2014-03-30	62.224	151.144	72	5.1
2015-07-06	62.130	150.789	71	4.9
2015-07-25	61.949	152.052	126	5.1
2015-07-29	59.894	153.196	119	6.3
2016-01-18	62.103	150.640	10	4.5
2016-01-24	59.719	153.168	107	4.6
2016-01-24	59.731	153.146	107	4.9
2016-01-24	59.620	153.339	126	7.1
2016-01-25	59.744	153.158	108	4.5
2016-01-28	59.699	153.166	107	4.6
2016-02-03	60.333	153.546	189	4.6
2016-02-09	59.788	152.975	108	4.5
2016-02-10	59.719	153.166	106	4.5
2016-02-10	59.713	153.154	106	4.6
2016-03-12	60.261	152.304	100	4.7
2017-01-26	62.008	152.390	142	4.5
2017-01-31	63.071	150.906	117	5.4
2017-03-02	59.579	152.655	78	5.3
2017-04-29	63.123	151.166	12	5.0
2017-05-07	60.183	151.680	67	5.0
2017-05-30	60.838	151.828	78	5.1
2017-08-11	60.067	152.477	96	4.8
2017-08-31	63.012	150.538	105	4.5
2017-10-19	59.745	153.132	102	4.8
2017-11-05	60.225	153.076	140	4.9
2017-11-27	60.555	147.430	17	5.1
2018-03-09	59.751	153.126	100	4.9
2018-07-01	63.068	150.797	117	4.9
2018-07-10	62.979	150.636	113	4.9

Date (YYYY-MM-DD)	Latitude (°N)	Longitude (°W)	Depth (km)	Magnitude (M_W)
2018-10-15	61.287	150.522	72	4.5
2018-11-21	59.955	153.266	143	5.5
2018-11-30	61.398	149.998	47	4.5
2018-11-30	61.479	149.923	37	4.5
2018-11-30	61.283	149.908	46	4.8
2018-11-30	61.384	150.080	38	4.9
2018-11-30	61.459	149.954	40	5.2
2018-11-30	61.282	149.957	41	5.5
2018-11-30	61.346	149.955	47	7.1
2018-12-01	61.473	149.898	34	4.5
2018-12-01	61.376	149.978	45	4.5
2018-12-01	61.483	149.936	51	4.9
2018-12-01	61.355	149.991	43	5.0
2018-12-02	61.325	149.901	52	4.5
2018-12-04	61.394	150.076	38	4.5
2018-12-05	61.323	150.053	42	4.5
2018-12-06	61.341	149.955	43	4.7
2018-12-09	61.420	149.837	41	4.7
2019-01-01	61.298	149.952	44	4.9
2019-01-11	61.471	149.899	50	4.5
2019-01-13	61.299	150.065	45	4.9
2019-01-23	61.503	150.237	46	4.5

Appendix C: Strong-motion Station Horizontal to Vertical Spectral Ratio (HVSR) Plots, where the black line and grey shading are the median HVSR results with the standard error and the red line indicates the average SSR of each station.

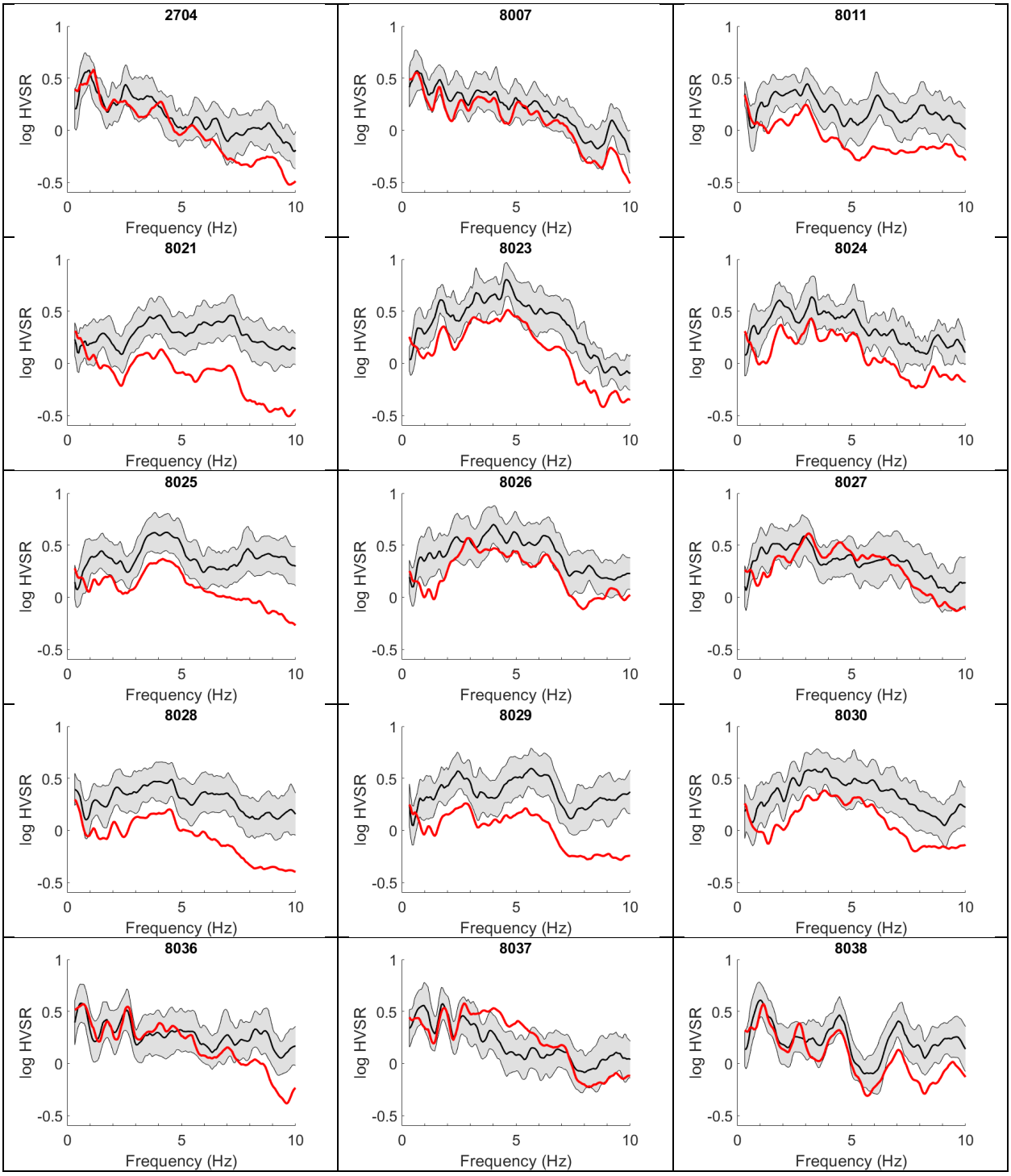

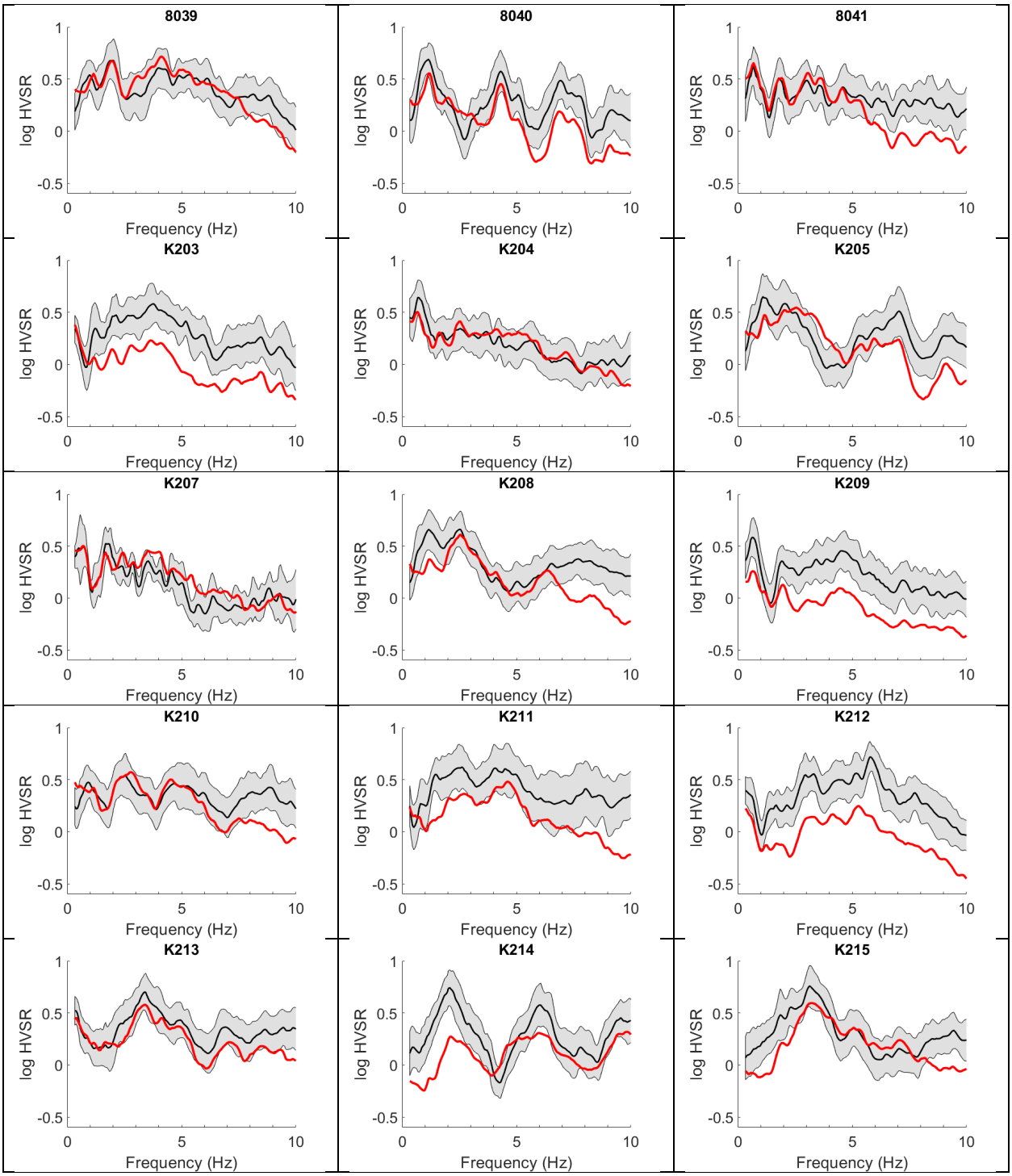
8039
8040
8041
K203
K204
K205
K207
K208
K209
K210
K211
K212
K213
K214
K215
log HVSR
Frequency (Hz)
1
0.5
0
-0.5
0
5
10

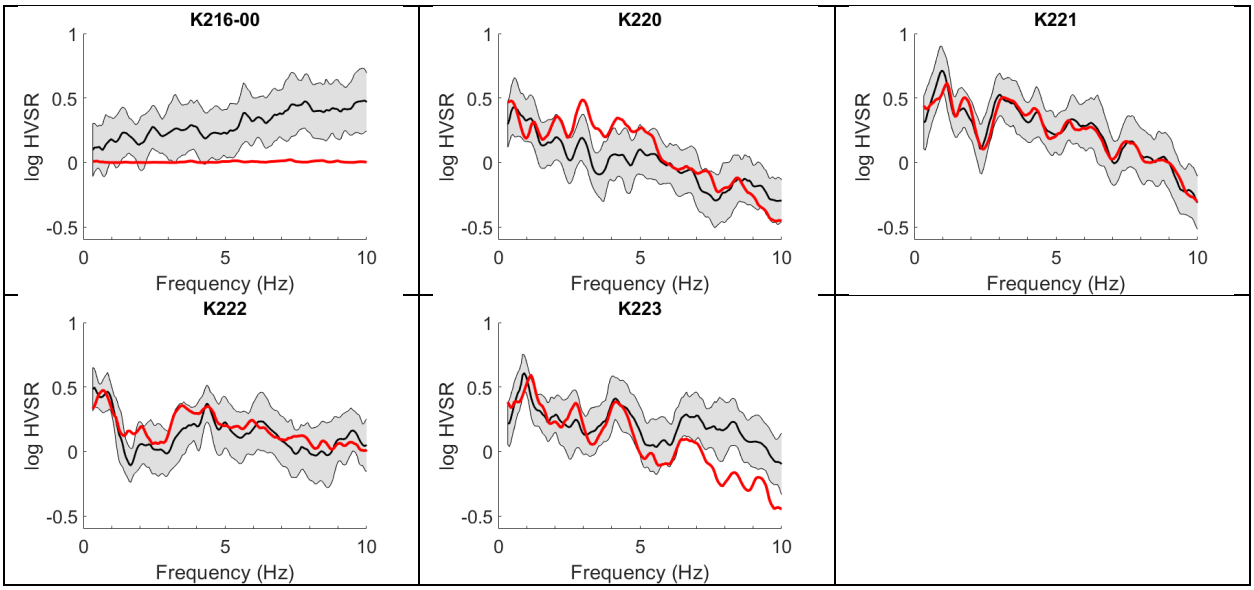
K216-00
K220
K221
K222
K223
log HVSR
Frequency (Hz)
1
0.5
0
-0.5
0
5
10

Appendix D: V_{S30} Data (Dutta et al. [39])

Site ID	Latitude (°N)	Longitude (°W)	V_{S30} (m/s)
An02	61.075	149.807	538
An03	61.114	149.820	420
An09	61.153	149.929	250
An10	61.189	150.015	315
An11	61.186	149.875	401
An12	61.191	149.824	499
An13	61.181	149.720	571
An14	61.210	149.909	253
An16	61.249	149.818	278
An17	61.223	149.725	453
An21	61.186	149.938	263
An22	61.137	149.890	380
S-07	61.155	149.897	313
S-22	61.112	149.805	504
S-38	61.215	149.763	448
S-39	61.098	149.832	514
S-43	61.203	149.795	451
S-55	61.220	149.785	408
S-66	61.131	149.830	445
S-69	61.170	149.873	376
S-73	61.197	149.890	404